



HAL
open science

Hydrophobization of Cellulose Nanocrystals for Aqueous Colloidal Suspensions and Gels

Rinat Nigmatullin, Marcus Johns, Juan Muñoz-García, Valeria Gabrielli, Julien Schmitt, Jesus Angulo, Yaroslav Khimyak, Janet Scott, Karen Edler, Stephen Eichhorn

► **To cite this version:**

Rinat Nigmatullin, Marcus Johns, Juan Muñoz-García, Valeria Gabrielli, Julien Schmitt, et al.. Hydrophobization of Cellulose Nanocrystals for Aqueous Colloidal Suspensions and Gels. *Biomacromolecules*, 2020, 21 (5), pp.1812-1823. 10.1021/acs.biomac.9b01721 . hal-03037583

HAL Id: hal-03037583

<https://hal.science/hal-03037583v1>

Submitted on 3 Dec 2020

HAL is a multi-disciplinary open access archive for the deposit and dissemination of scientific research documents, whether they are published or not. The documents may come from teaching and research institutions in France or abroad, or from public or private research centers.

L'archive ouverte pluridisciplinaire **HAL**, est destinée au dépôt et à la diffusion de documents scientifiques de niveau recherche, publiés ou non, émanant des établissements d'enseignement et de recherche français ou étrangers, des laboratoires publics ou privés.

Hydrophobization of Cellulose Nanocrystals for Aqueous Colloidal Suspensions and Gels

Rinat Nigmatullin,* Marcus A. Johns, Juan C. Muñoz-García, Valeria Gabrielli, Julien Schmitt, Jesús Angulo, Yaroslav Z. Khimyak, Janet L. Scott, Karen J. Edler, and Stephen J. Eichhorn*



Cite This: <https://dx.doi.org/10.1021/acs.biomac.9b01721>



Read Online

ACCESS |



Metrics & More

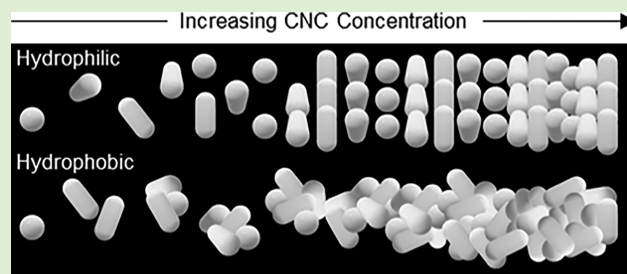


Article Recommendations



Supporting Information

ABSTRACT: Surface hydrophobization of cellulose nanomaterials has been used in the development of nanofiller-reinforced polymer composites and formulations based on Pickering emulsions. Despite the well-known effect of hydrophobic domains on self-assembly or association of water-soluble polymer amphiphiles, very few studies have addressed the behavior of hydrophobized cellulose nanomaterials in aqueous media. In this study, we investigate the properties of hydrophobized cellulose nanocrystals (CNCs) and their self-assembly and amphiphilic properties in suspensions and gels. CNCs of different hydrophobicity were synthesized from sulfated CNCs by coupling primary alkylamines of different alkyl chain lengths (6, 8, and 12 carbon atoms). The synthetic route permitted the retention of surface charge, ensuring good colloidal stability of hydrophobized CNCs in aqueous suspensions. We compare surface properties (surface charge, ζ potential), hydrophobicity (water contact angle, microenvironment probing using pyrene fluorescence emission), and surface activity (tensiometry) of different hydrophobized CNCs and hydrophilic CNCs. Association of hydrophobized CNCs driven by hydrophobic effects is confirmed by X-ray scattering (SAXS) and autofluorescent spectroscopy experiments. As a result of CNC association, CNC suspensions/gels can be produced with a wide range of rheological properties depending on the hydrophobic/hydrophilic balance. In particular, sol–gel transitions for hydrophobized CNCs occur at lower concentrations than hydrophilic CNCs, and more robust gels are formed by hydrophobized CNCs. Our work illustrates that amphiphilic CNCs can complement associative polymers as modifiers of rheological properties of water-based systems.



INTRODUCTION

Advanced functional materials and devices based on nanomaterials capitalize on the unique properties of the nanoparticles used as building elements.^{1,2} A vast diversity of potential applications has generated demand for nanoparticles of different shapes (spheres, rods, fibrils, platelets, etc.), sizes, and chemical compositions. Progress in the chemical synthesis of nanoparticles has been complemented by their isolation or construction from materials of biological origin.^{3,4} These latter approaches provide sustainable routes for nanoparticle generation. In this respect, nanomaterial isolation from various cellulose-rich biomass (wood, plants, algae, bacterial biomass, etc.) becomes an established approach to generate highly crystalline nanoparticles of high aspect ratio with diameters from 5 to 100 nm and lengths from tens to several hundred nanometers.^{5,6} The high crystallinity of cellulose nanomaterials (CNMs) defines their exceptional strength and stiffness. Also, CNM morphology, reactivity, and topochemistry provide a versatile platform for advanced functional materials.

The success in CNM utilization as building blocks largely depends on their directed or self-assembly in isolation, or in combination with other components into specific structures.^{7–9} Assembly of nanoparticles requires certain chemical

motifs on their surface. For example, sulfated cellulose nanocrystals (CNCs) form stable chiral nematic liquid crystalline phases,¹⁰ while low surface charge CNCs tend to assemble at the liquid–liquid interface due to the hydrophobic, or hydrophilic, nature of their different crystal faces.¹¹ Therefore, surface modification or functionalization is an important, very often indispensable, step toward functional nanomaterials. On the molecular level, CNMs contain reactive hydroxyl groups, which enable changes in surface properties via very diverse and well-established chemical pathways.^{12,13}

Hydrophobization of CNMs has been well-documented in the literature. Various chemical routes have been employed for functionalization of CNM surfaces with hydrophobic domains via covalent binding. CNM hydrophobization has been conducted via silylation using alkyl dimethylchlorosilanes with various lengths of alkyl groups,^{14–16} esterification with acyl chlorides,^{17,18} and urethanization using hydrophobic isocya-

Special Issue: Anselme Payen Award Special Issue

Received: December 13, 2019

Revised: January 23, 2020

Published: January 25, 2020

nates.^{19,20} These one-step modification methods involve water-sensitive reactants and, therefore, require organic solvents for the reactions. Moreover, for these chemical routes there is a risk of a reduction in the crystallinity of the cellulose, or even obtaining soluble products if the degree of functionalization is too high. Graft copolymerization has also been used for CNC hydrophobization.^{21,22} Water-based hydrophobization of anionic CNMs (sulfated CNCs, TEMPO-oxidized CNCs) has been achieved via ionic interactions with cationic surfactants containing long alkyl groups.^{23–34} This is a simple approach for the hydrophobization of CNMs. However, binding is reversible, and modifying surfactants can be released from the CNM surface. Reductive amination is another modification route for CNMs, which can be conducted in aqueous media.³⁵ In this case, CNMs are activated by periodate oxidation leading to partial transformation into dialdehyde cellulose, which is followed by a reaction of the formed aldehyde groups with primary amines. Unlike ionic binding, reductive amination results in covalent binding of the modifying agent, which can be a hydrophobic amine. For example, modification with butylamine isomers using this route enabled isolation of hydrophobized CNCs from Kraft pulp without acid hydrolysis.^{36,37} Preactivation of CNMs can also be omitted since cellulose chains contain aldehyde groups at the reducing end.³⁸ CNM activation for covalent binding of hydrophobic amines has been achieved by coating CNCs with tannic acid as a reactive primer.³⁹ For this approach, all modifications steps were also conducted in aqueous media.

The interest in hydrophobic derivatives of CNMs has mainly been driven by the potential applications in two fields: polymer nanocomposites and emulsion stabilization. The exceptional strength and stiffness of CNMs have also raised great expectations for the development of polymer nanocomposites.⁴⁰ However, most synthetic polymers are hydrophobic materials, which results in poor wettability of CNMs and weak adhesion with the polymer matrix. Thus, surface hydrophobization has been considered as a means for improving the compatibility between nanocomposite components.^{18,19,32,41–44} Emulsion stabilization by unmodified CNMs has also given impetus for functionalization of CNMs with hydrophobic domains for the enhancement of emulsifying properties.^{11,17,28,29,31,36–38} However, the literature lacks studies focused on hydrophobized CNMs in aqueous systems, despite the fact that water-soluble polymers with moderate contents of hydrophobic moieties are widely used as viscosity modifiers in various aqueous industrial formulations such as paints, pharmaceuticals, cosmetics, foods, etc.^{45–47} These applications are based on the ability of such polymers to form a transient network due to reversible association between the hydrophobic groups. Recently it was demonstrated that properly adjusted hydrophobization of charged CNCs resulted in derivatized CNCs forming stable aqueous suspensions.^{21,48} Such associative CNCs undergo sol to gel transitions in aqueous suspensions at significantly lower concentrations compared with their hydrophilic counterparts. Gels of hydrophobized CNCs exhibited higher viscosities and stronger elastic responses, which was attributed to the formation of transient networks driven by hydrophobic effects. With these hydrophobized CNCs, hydrophobic effects can be utilized for the design of hybrid systems consisting of nanoparticles and other water-soluble polymers as it was demonstrated in combinations with starch, a helical polysaccharide,⁴⁸ and thermally responsive hydroxypropyl methyl cellulose.⁴⁹ Thus,

hydrophobized CNMs have a potential to complement a group of associative materials for their use in water-based systems.

This study reports the properties of aqueous colloidal systems with hydrophobized CNCs, with a focus on the impact of hydrophobic effects on CNC association and gelation in aqueous media. A synthetic route based on reductive amination was adopted for CNC hydrophobization with the intention to use water-based modification leading to covalent binding of hydrophobic groups of various length to the CNC surface. Detailed characterization of these hydrophobized CNCs in aqueous suspensions was obtained compared to the parent hydrophilic CNCs by surface tensiometry, electrophoretic light scattering, fluorescence anisotropy, autofluorescent spectroscopy, small-angle X-ray scattering (SAXS), oscillatory rheology, and steady-shear viscometry. We demonstrate that self-association driven by hydrophobic effects induces sol–gel transformation at lower concentrations of hydrophobized CNCs and leads to the formation of more robust gels. Thus, amphiphilic derivatives of CNCs, or other CNMs, could further expand the selection of associative polymers to offer more flexibility in modifications of rheological properties of water-based systems.

EXPERIMENTAL METHODS

Chemical Modification of CNCs. The CNC surfaces were modified by binding alkylamines of different chain length, hexylamine (C₆–CNCs), octylamine (C₈–CNCs), and dodecylamine (C₁₂–CNCs) according to a procedure previously described.⁴⁹ First, the CNC surfaces were activated by oxidation in aqueous suspension (1.6 wt %) using sodium periodate (1.68 mmol of NaIO₄ per 1 g of CNC) at room temperature for 48 h. After oxidation, the CNC suspension was dialyzed against deionized (DI) water for 24 h using a cellulose membrane with a molecular cutoff of ~14 kDa. Alkylamines (7.7 mmol per 1 g of CNCs) were added to the purified suspension of oxidized CNCs. Reaction of oxidized CNCs with alkylamines was first conducted at 45 °C for 3 h, and then for a further 21 h at room temperature after adding NaBH₃CN (40 mM). Modified CNCs were purified using centrifugation and a 2 wt % NaCl solution in an isopropanol/water mixture (50/50 v/v) as a washing solvent. Finally, modified CNCs were redispersed and dialyzed in and against DI water. The purified modified CNC suspensions were concentrated by allowing water evaporation through the dialysis membrane. To evaluate noncovalent binding of alkylamines to the CNCs' surface, the oxidation step was omitted, and CNC suspensions were directly treated with octylamine. Reagent ratio and purification steps were the same as in the preparation of covalently modified CNCs. All modified CNCs were stored as never-dried materials.

Nuclear Magnetic Resonance (NMR) Spectroscopy. Solid-state NMR experiments were performed using a Bruker Avance III spectrometer equipped with a 4 mm triple resonance probe operating at frequencies of 300.13 MHz (¹H) and 75.47 MHz (¹³C). C₆–CNC, C₈–CNC, and C₁₂–CNC powders were tightly packed in an 80 μL rotor and spun at a MAS rate of 12 kHz. ¹H–¹³C CP/MAS NMR spectra (referenced with respect to TMS) were acquired at room temperature using 20k scans, a recycle delay of 10 s, and a contact time of 1 ms. It should be noted that it has been previously shown that ¹H–¹³C CP/MAS NMR spectra of cellulose can be considered quantitative for CP contact times larger than 600 μs.⁵⁰ CNC specific surface area and degree of functionalization were calculated from the peaks of C6 located in the interior and surface domains as described in the SI.

Characterization of Surface Properties of CNCs. The content of sulfate groups on the surface of the CNCs was determined by conductometric titration⁵¹ using 20 mL of a CNC suspension with a concentration of ~3 mg mL⁻¹. A 1.5 mM NaOH solution was used as the titrant. The conductivity values were corrected for dilution effects. The ζ potentials of CNCs were measured with a Zetasizer Nano ZS

193 instrument (Malvern Instruments Ltd.) using 0.5 mg mL⁻¹ CNC
 194 suspensions in DI water. ζ potential was estimated as an average of 15
 195 measurements. Water contact angle measurements were conducted to
 196 estimate hydrophobicity of CNCs. Films of CNCs were prepared by
 197 drying 1 wt % suspensions on glass slides. The automatic dispenser of
 198 a DSA100 drop shape analyzer (Krüss, Germany) was used to inject a
 199 droplet of known volume of 2 μ L on a substrate surface. ADVANCE
 200 software (Krüss, Germany) was used to analyze images of sessile
 201 drops and calculate static water contact angles.

202 **Characterization of CNC Suspensions.** Surface tension of CNC
 203 aqueous suspensions was measured using an advanced surface
 204 tensiometer K100 (Krüss, Germany) equipped with a standard
 205 measuring probe (PL01) and by the Wilhelmy plate method.
 206 Measurements at different CNC concentrations were performed by
 207 automatic serial dilutions of CNC suspensions with an initial
 208 concentration of 7000 mg L⁻¹ using two microdispensers
 209 (DS0810). Pyrene fluorescence emission was used for probing the
 210 microenvironment in CNC suspensions. Aliquots (100 μ L) of 0.4
 211 mM pyrene solution in ethanol were dispensed into 7 mL glass vials
 212 and allowed to dry at room temperature in the dark. A 4 mL portion
 213 of CNC suspensions with different concentrations was added to the
 214 vials resulting in a 10⁻⁵ M pyrene concentration. The fluorescence
 215 emission spectra of the pyrene probe at various CNC concentrations
 216 were recorded from 340 to 500 nm with 334 nm excitation
 217 wavelength by a FluoroMax-4 fluorescence spectrometer (HORIBA
 218 Instruments). The slit settings for excitation and emission were 2 and
 219 1 nm, respectively.

220 **SAXS Measurements.** Suspensions of unmodified and modified
 221 CNCs at different concentrations (ranging from 1 to 10 wt % for
 222 unmodified CNCs, 0.1 to 6 wt % for C8-CNCs) and suspensions in
 223 the presence of 0.1 M KCl were loaded in 1.5 mm diameter
 224 capillaries, sealed, and measured using small-angle X-ray scattering
 225 (SAXS). Part of the measurements was done at the I22 beamline of
 226 the Diamond Light Source (Didcot, Oxfordshire), operating at a
 227 wavelength $\lambda = 1 \text{ \AA}$ ($E = 12.4 \text{ keV}$), giving the following q -range: $4 \times$
 228 $10^{-2} < q < 0.25 \text{ \AA}^{-1}$. The data were collected using a Pilatus P3-2 M
 229 instrument (Silicon hybrid pixel detector, DECTRIS) averaging 10
 230 frames of 100 ms exposure time each. Complementary measurements
 231 were done using a SAXSLab Ganesha 300XL instrument (SAXSLAB,
 232 ApS, Skovlunde, Denmark), operated at a wavelength $\lambda = 1.54 \text{ \AA}$ and
 233 equipped with a moveable Pilatus 300 K 2D detector. A similar q -
 234 range as Diamond ($4 \times 10^{-2} < q < 0.25 \text{ \AA}^{-1}$) was obtained by
 235 merging the patterns obtained at 3 different sample-detector
 236 distances and recorded for 1800, 3600, and 7200 s, respectively.
 237 For both I22 and Ganesha data, signals of the solvent and capillary
 238 were subtracted, and Lupolen was used for an absolute scaling
 239 calibration.

240 SAXS patterns were fitted using a model of interacting stiff rods.
 241 The rods are characterized by an elliptical cross-section of minor and
 242 major radii R_{\min} and R_{\max} (both in nm), respectively, and a length L
 243 (in nm). Interactions between CNCs were modeled using the PRISM
 244 model which depends on the strength of interaction via the so-called
 245 "excluded volume parameter" ν_{RPA} (>0 for repulsive interaction
 246 between CNC) and a "hard-sphere" radius R_{cq} ($\geq R_{\max}$), correspond-
 247 ing to the section radius along the rods which is not accessible to any
 248 other rod. A full description of this model and its use for TEMPO-
 249 oxidized cellulose nanofibrils has previously been reported.⁵²

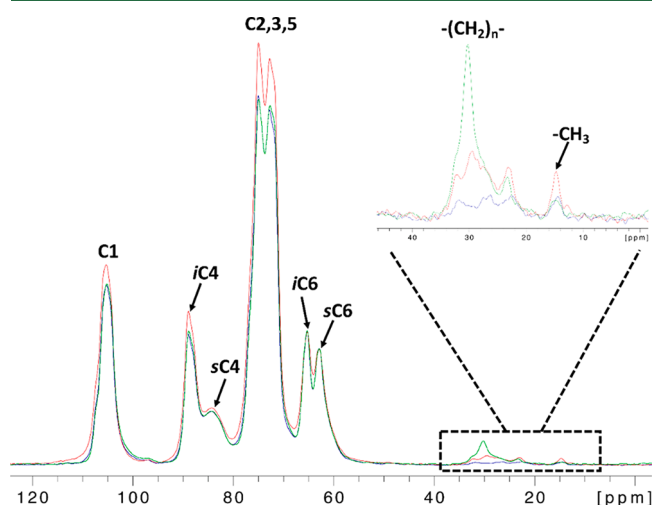
250 **Rheological Measurements.** A Discovery HR-1 rotational
 251 rheometer (TA Instrument) operating with a stainless steel cone
 252 plate geometry (diameter 40 mm, angle 4°) and a Peltier plate for
 253 temperature control was used for the rheological measurements of the
 254 CNC suspensions and gels. An isothermal dynamic amplitude sweep
 255 was performed to determine the linear viscoelastic (LVE) region and
 256 confirmed that 1.5% strain was inside the LVE region for all tested
 257 samples. Frequency sweeps were conducted in strain-controlled mode
 258 at 1.5% strain for an angular frequency range from 0.4 to 100 rad s⁻¹.
 259 Steady-state shear viscosity was measured within the shear rate range
 260 0.01–100 s⁻¹.

RESULTS AND DISCUSSION

261

262 **Surface Modification of CNCs.** With the aim to use water
 263 as a medium for CNC modification, a reductive amination of
 264 aldehyde groups with primary amines has been selected as the
 265 chemical route for hydrophobization. CNCs produced by
 266 hydrolysis in concentrated solutions of sulfuric acid are, in fact,
 267 functionalized nanoparticles due to the formation of sulfate
 268 half-ester groups on the CNC surface. As a result, the covalent
 269 linkage of alkylamine to the CNC surface can be accompanied
 270 by ionic binding of alkylamines due to interaction between
 271 sulfate and amine groups. Although ionic binding has been
 272 used for CNC hydrophobization in some applications,^{23–34} it
 273 is reversible and potentially can lead to undesired or even
 274 harmful release of a cationic modifier. Therefore, the
 275 procedure for CNC modification was designed to minimize
 276 ionic binding. To avoid the establishment of ionic interactions
 277 between protonated amines, the pH of the reaction media was
 278 maintained slightly alkaline due to dissolved alkylamines.
 279 Purification of modified CNCs was conducted by washing in a
 280 water/isopropanol (50/50 vol/vol) mixture which ensures the
 281 dissolution of alkylamines.

282 The presence of alkyl chains in modified CNCs was
 283 confirmed by ¹H–¹³C CP/MAS NMR experiments (Figure
 284 1). To demonstrate that the alkyl moieties were covalently



285 **Figure 1.** Typical ¹H–¹³C CP/MAS NMR spectra of covalently
 286 hydrophobized C₆–CNC (blue), C₈–CNC (red, from ref 48), and
 287 C₁₂–CNC (green) powders acquired at 12 kHz MAS rate at room
 288 temperature. The ¹³C peaks corresponding to the alkyl moieties are
 289 magnified in the inset. The three spectra are scaled to match the same
 290 intensity for the sC6 peak.

291 attached to CNCs, and not just physically adsorbed, we also
 292 carried out ¹H and ¹H–¹³C CP/MAS NMR experiments for a
 293 noncovalently modified hydrophobized CNC, namely, C₈–
 294 CNC_{NC} (SI, Figure S1). Interestingly, while the ¹H NMR
 295 spectrum of noncovalently modified C₈–CNC_{NC} clearly
 296 showed the presence of alkyl groups in the material, no alkyl
 297 peaks were detected in the ¹H–¹³C CP/MAS experiment (10–
 298 50 ppm; SI, Figure S1). It is most likely that the alkyl chains in
 299 this material are too mobile to cross-polarize effectively and,
 300 hence, are not covalently attached to the CNC surface. The
 301 ¹H–¹³C CP/MAS NMR can be used to probe for covalent
 302 surface functionalization of CNCs, and we have demonstrated

297 that covalent hydrophobization was successful for C₆–, C₈–
298 and C₁₂–CNC samples (Figure 1).

299 The spectral deconvolution of the *i*C6 and *s*C6 peaks from
300 ¹H–¹³C CP/MAS NMR spectra enabled us to estimate the
301 surface areas (eqs S1 and S2) of nonmodified CNC, C₆–CNC,
302 and C₁₂–CNC (Table 1; SI, Figures S2 and S3). Similar

Table 1. Summary of the Calculated Parameters Obtained from Spectral Deconvolution of *i*C6 and *s*C6 Peaks of the ¹H ¹³C CP Spectra of Covalently Hydrophobized C₆–CNC, C₈–CNC, and C₁₂–CNC Powders

	CNC	C ₆ –CNC	C ₈ –CNC ^a	C ₁₂ –CNC
<i>q</i>	0.57 ± 0.02	0.49 ± 0.02	0.52 ± 0.02	0.51 ± 0.02
$\sigma_{\text{fbpril}}^{\text{fbpril}}$ [m ² g ⁻¹]	805 ± 40	674 ± 34	693 ± 35	701 ± 35
DSF [%]	n/a ^b	3.6 ± 0.4	4.1 ± 0.4	2.6 ± 0.3

^aFrom Nigmatullin et al.⁴⁸ ^bn/a: not applicable.

303 surface areas were obtained for C₆–CNC and C₁₂–CNC,
304 which are comparable to the value previously reported for C₈–
305 CNC⁴⁸ (within the experimental error, Table 1). In contrast,
306 nonmodified CNC showed a surface area significantly larger
307 than the three hydrophobized CNCs (SI, Figures S2). From
308 the same ¹H–¹³C CP/MAS NMR, the spectral deconvolution
309 of the alkyl peaks of C₆–CNC and C₁₂–CNC (SI, Figure S3)
310 was used to calculate the degree of surface functionalization
311 (DSF, eq S3) of modified CNCs. A DSF of 3.6 ± 0.4% and 2.6
312 ± 0.3% was determined for C₆–CNC and C₁₂–CNC,
313 respectively (Table 1). Hence, the DSF of C₆–CNC is
314 comparable, within the experimental error, to the value
315 reported previously for C₈–CNC,⁴⁸ whereas degree of
316 functionalization was slightly less efficient for C₁₂–CNC. It
317 might be caused by lower solubility of dodecylamine compared
318 with hexyl- and octylamine.

319 **Physicochemical and Surface Properties of Hydro-**
320 **phobized CNCs.** The CNCs used in this study were
321 produced by hydrolysis in concentrated sulfuric acid solution.
322 It is well-known that such an isolation of CNCs results in
323 highly charged rod-shaped nanoparticles due to esterification
324 of cellulose hydroxyl groups with sulfuric acid.^{51,53} The
325 –SO₃H[−] group content for CNCs used in this study was
326 around 235 mmol kg^{−1} of CNC determined from conducto-
327 metric titration. This results in nanoparticles with high
328 negative surface charge as characterized by ζ potential, ca.
329 −48 mV (Table 2), which plays a crucial role in their colloidal

Table 2. Surface Properties of Initial and Hydrophobized CNCs

CNC type	–SO ₃ H [−] , mmol kg ^{−1}	ζ potential, mV	water contact angle, deg
CNCs	235 ± 30	−48.3 ± 0.5	40.6 ± 2.5
C ₆ –CNCs	112 ± 18	−41.4 ± 1.2	59.5 ± 1.3
C ₈ –CNCs	118 ± 8	−44.1 ± 0.8	62.6 ± 2.6
C ₁₂ –CNCs	131 ± 13	−43.3 ± 0.6	66.0 ± 0.5

330 stability.^{54,55} Hydrophobization of the CNCs via binding of
331 alkylamines was accompanied by a decrease of the sulfate half-
332 ester group content by almost half (Table 2). Nevertheless, the
333 ζ potential, the determination of which is based on the
334 electrophoretic mobility of the nanoparticles, decreased by
335 only a few units for hydrophobized CNCs. Only small

variations in sulfate group content and ζ potentials were
observed for CNCs modified with alkylamines of different
lengths.

Sulfate half-esters in cellulose derivatives give several
characteristic Raman bands (Zhang, Brendler et al. 2010).
The Raman bands located at ~825 and ~1270 cm^{−1},
attributed to the C–O–S stretching vibration and the O=
S=O asymmetric stretching vibrations, respectively, decreased
after CNC oxidation with sodium periodate (SI, Figure S4).
This confirms that partial desulfation of CNCs took place
during the oxidation stage. Despite this desulfation, a
significant fraction of sulfate half-ester groups remained intact
in hydrophobized CNCs. The absolute value of ζ potentials of
modified CNCs did not decrease below ~40 mV which is
usually considered to be sufficient for high nanoparticle
colloidal stability in aqueous suspensions.

To confirm the introduction of hydrophobic domains to the
surface, water contact angles were measured for CNC films
prepared by drying 1 wt % suspensions on glass slides. The
water contact angle for the unmodified CNC film was ~40°
demonstrating wettability with water and thereby CNC
hydrophilicity (Table 1 and SI, Figure S5). However,
wettability of films made of modified CNCs notably decreased,
and water contact angles rose to >60°. A gradual increase in
water contact angle was observed with an increase in
alkylamine chain length. Thus, modified CNCs are more
hydrophobic than CNCs, and hydrophobicity of modified
CNCs increased in the following order: C₆–CNCs < C₈–
CNCs < C₁₂–CNCs.

Binding hydrophobic groups to the CNC surface is expected
to change the microenvironment in aqueous CNC dispersions,
similar to surfactant layers adsorbed onto particle surfaces.⁵⁶
Pyrene, the fluorescence emission of which is sensitive to the
solvent polarity, is a common probe in micellar systems and
has been used to characterize microenvironments at inter-
faces.⁵⁷ Figure 2 presents the changes in the intensity ratios for
the third (*I*₃) and first (*I*₁) vibronic bands of pyrene fluorescent
emission at 382 and 370 nm, respectively with concentration
for different modified CNCs. Hydrophilic unmodified CNCs

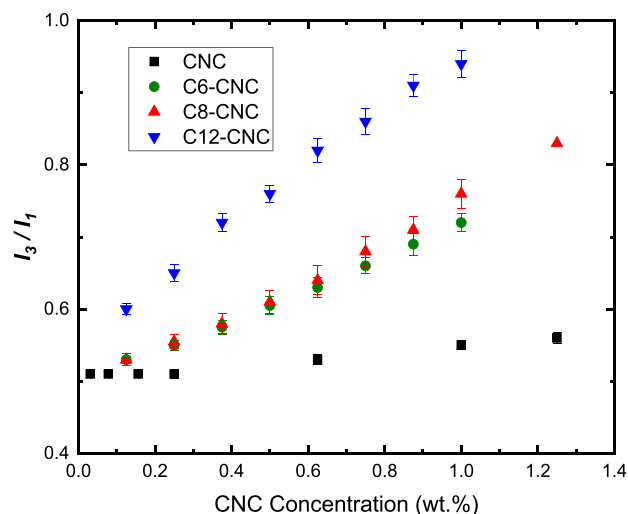


Figure 2. Change in the pyrene fluorescent emission intensity ratio *I*₃/*I*₁ in aqueous suspensions of unmodified (CNC) and modified CNCs (C₆–CNC, C₈–CNC, C₁₂–CNC) with a variation in the concentration of CNCs.

375 had very little effect on the pyrene fluorescence response, with
 376 I_3/I_1 ratios not exceeding 0.56, a value characteristic for water.
 377 Similar values were observed for modified CNCs when their
 378 concentrations were below 0.25 wt %. Thus, under these
 379 conditions, pyrene was in a polar, hydrophilic microenviron-
 380 ment. In contrast, I_3/I_1 values for modified CNCs monotonically
 381 increased with concentration providing evidence that the
 382 microenvironment became increasingly nonpolar in aqueous
 383 dispersions of modified CNCs. In a similar trend to contact
 384 angle measurements, C_{12} -CNCs generated the most nonpolar
 385 microenvironment followed by C_8 - and C_6 -CNCs. I_3/I_1
 386 values for modified CNCs ranged from 0.51 to 0.94, which
 387 are typical values for aqueous micellar systems.^{56,58} However,
 388 the concentration dependence of I_3/I_1 ratios in surfactant
 389 systems has an S-shaped pattern with a sharp increase around
 390 the critical micellar concentration due to the increase of pyrene
 391 solubilization in micelles. The observed monotonic increase in
 392 I_3/I_1 ratio with increasing modified CNC concentration is
 393 probably due to the combination of two different mechanisms
 394 of pyrene solubilization: solubilization at interfaces of CNCs
 395 containing hydrophobic domains and solubilization in a
 396 volume formed via aggregation driven by hydrophobic effects.
 397 The latter is similar to pyrene solubilization in micelles, while
 398 the former has been reported for dispersion of hydrophobized
 399 particles or particles with adsorbed surfactants.^{56,57}
 400 Characterization of surface properties of modified CNCs
 401 provides evidence that both hydrophilic and hydrophobic
 402 domains are present on the surface of modified CNCs. As a
 403 result, modified CNCs exhibited surface activity and decrease
 404 interfacial tension (Figure 3). Unmodified CNCs did not

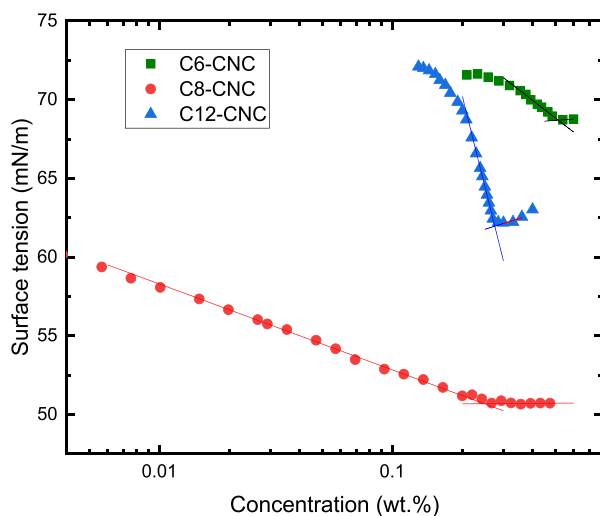


Figure 3. Dependence of modified CNC surface tension on concentration. Solid lines are linear fits of a plateau region and linearly dependent regions preceding the plateau. Critical aggregation concentrations (CACs) ca. 0.51, 0.25, and 0.27 wt % were determined for C_6 -, C_8 -, and C_{12} -CNCs, respectively, as the intersection between these linear fits.

405 however induce a decrease in the interfacial tension in
 406 suspensions with concentrations up to 0.8 wt % (data not
 407 shown). However, there appeared to be no direct correlation
 408 between the length of alkyl chains attached to the CNC surface
 409 and surface activity. The highest decrease in surface tension, to
 410 $\sim 51 \text{ mN m}^{-1}$, was observed for the C_8 -CNCs suspension at
 411 concentrations higher than 0.25 wt %. Despite showing higher

hydrophobicity, demonstrated by contact angle and pyrene
 probe measurements, C_{12} -CNCs caused only a moderate
 decrease (to $\sim 62 \text{ mN m}^{-1}$) in surface tension. Stronger
 hydrophobic effects in C_{12} -CNCs suspensions might induce
 association of the C_{12} -CNCs and decrease the content of
 individualized CNCs in the suspension. Since individualized
 CNCs are expected to be drawn to the interface, C_{12} -CNCs
 had lower surface activity in comparison with C_8 -CNCs. The
 lowest surface activity was exhibited by C_6 -CNCs, suggesting
 that the surface charge and other hydrophilic cellulose groups
 prevail over the hydrophobic domains, resulting in their
 dispersion in the water bulk rather than being drawn to the
 water interface. All three hydrophobized CNCs showed
 concentration dependence typical for amphiphiles, exhibiting
 concentration dependent segments at low concentrations, and
 regions of constant surface tension when concentration
 exceeded a critical value. A critical aggregation concentration
 (CAC), defined as the onset of a steady state value of surface
 tension, is associated with the formation of aggregated
 structures in the bulk of the solution. The CAC values for
 C_6 -, C_8 -, and C_{12} -CNCs were found to be ca. 0.51, 0.25, and
 0.27 wt %, respectively (Table 3). There were no detectable
 changes in the form of the pyrene emission curves (Figure 2)
 around these CAC values, confirming the hypothesis that
 different mechanisms are involved in pyrene solubilization in
 these systems. This is unlike for micellar systems where pyrene
 is mostly solubilized in micelles with a drastic increase in the
 I_3/I_1 ratio at concentrations close to the critical micellar
 concentration.

Structure of Aqueous CNC Suspensions. To probe the
 effect of hydrophobization on CNC interaction in aqueous
 media, multichannel confocal laser scanning spectroscopy
 (MCLSS) and SAXS experiments were conducted for
 unmodified and modified CNC suspensions at various
 concentrations. The former technique is based on the
 autofluorescence of cellulose materials. Recently it was
 demonstrated that the autofluorescence of cellulose could be
 used to track microfibrils and nanocrystals in composite
 structures.^{44,59} Two autofluorescent emission bands were
 found to be dominant: one at 463.5–472.5 nm (herein
 referred to as the 468 nm band) and one at 499.5–508.5 nm
 (herein referred to as the 504 nm band). We theorize that the
 468 nm band is related to intraparticle forces (hydrogen
 bonding, van der Waals forces, and electrostatic forces), while
 the 504 nm band is related to those associated with
 interparticle interactions due to an expected lower excita-
 tion–emission conversion efficiency. To confirm this, the ratio
 between the 468 and 504 nm bands was tracked as the
 concentration of CNCs was increased from 0.1 to 11 wt %
 (Figure 4 and SI, Figure S6). As the concentration increases,
 the ratio between the two bands decreases, suggesting an
 increase in the intercrystal interactions. Taking the initial and
 final gradients of an exponential curve according to the
 equation

$$y = Ae^{(1-Bx)} + C \quad (1)$$

fitted to the data, where A , B , and C are constants (see Table 3
 for fit data), an interception point for unmodified CNCs is
 3.28 wt % (Table 3), which falls within the range at which
 chiral nematic phases are known to form for CNC
 suspensions;^{60,61} this confirms the fluorescent ratio depend-
 ence on CNC interaction. Hydrophobization of the CNCs

Table 3. Select Data for CNC and Modified CNC Suspensions As Determined by Surface Tension Measurements and Exponential Curves Fitted to MCLSS Data

CNM	CNCs	C ₆ -CNCs	C ₈ -CNCs	C ₁₂ -CNCs
CAC [wt %]		0.51	0.25	0.27
MCLSS interception point [wt %]	3.28 ± 0.09	1.40 ± 0.77	0.16 ± 0.00	0.25 ± 0.01
468:504 nm ratio [a.u.] (0 wt %)	1.30 ± 0.01	1.20 ± 0.01	1.30 ± 0.02	1.14 ± 0.00
468:504 nm ratio [a.u.] (100 wt %)	0.94 ± 0.00	1.23 ± 0.00	1.05 ± 0.00	1.04 ± 0.00

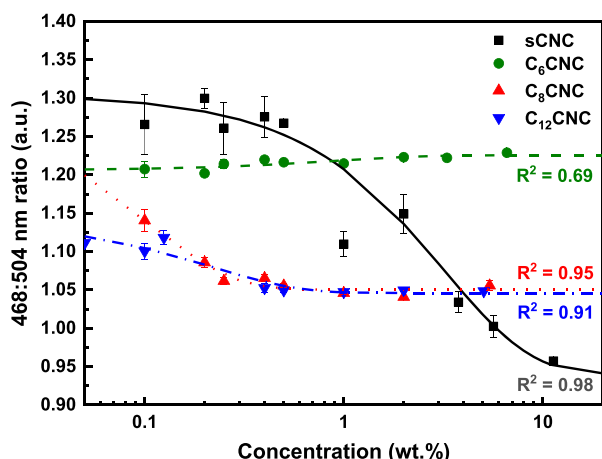


Figure 4. Effect of CNM concentration on ratio of emission intensity at 468 nm (associated with intracrystal fluorescence) and 504 nm (associated with intercrystal fluorescence). Exponential curves (eq 1) fitted for each data series. Error bars: \pm SE $N = 1$, $n = 3$.

473 results in their aggregation, as inferred from the interception
474 point, at lower concentrations than the hydrophilic CNCs
475 (Table 3) with the chain length series ($C_8 < C_{12} < C_6$)
476 matching that observed in surface tension experiments.

477 Further information on the nature of the interactions
478 between the hydrophobic CNCs may also be obtained from
479 the absolute 468:504 nm emission ratio values at theoretical
480 concentrations of 0 and 100 wt %. Unlike the other materials,
481 the C₆-CNCs exhibit an increase in the emission ratio as the
482 concentration increases. We theorize that the secondary amine
483 groups present, formed as a result of alkylamine coupling,
484 interact with the sulfate half-ester groups present on the CNC
485 surface. This results in a hypsochromic (blue) shift in the
486 spectrum and an increase in the emission intensity (SI, Figures

S6 and S7). We confirm that this is feasible by observing a
487 similar shift when a CNC gel is combined with a chitosan
488 solution (SI, Figure S8). In contrast, the lengths of the C8 and
489 C12 carbon chains inhibit this interaction, resulting in the
490 typical increase in the 504 nm band upon increasing
491 concentration.

492 From SAXS experiments (Figure 5 and SI, Figures S9 and
493 S10), unmodified CNC rods (Figure 5a) are found to have an
494 elliptical cross-section ($R_{\min} = 1.6 \pm 0.1$ and $R_{\max} = 15.0 \pm 0.1$
495 nm) and a length L fixed at ~ 110 nm in agreement with TEM
496 measurements. With increasing concentration, a growing
497 correlation peak emerges. This peak sharpens with concentra-
498 tion and moves toward larger q values (around $q \sim 0.015$
499 \AA^{-1} at 10 wt %). This correlation peak is due to increased
500 excluded volume interactions between unmodified CNCs and
501 is modeled using the PRISM model. From the fits, two
502 parameters are extracted: excluded volume parameter, ν_{RPA} ,
503 which is dependent on the interacting rod concentration, and
504 the radius of excluded volume, R_{cyl} , associated with the
505 intercylinder distance in concentrated regimes (Figure 6). ν_{RPA}
506 was found to increase linearly with concentration, as is
507 expected from increasing particle–particle interactions, due to
508 the electrostatic repulsion between the charged nanorods. On
509 the other hand, the local excluded volume parameter R_{cyl}
510 decreased with concentration, indicating a denser packing of
511 CNCs. The decrease is pronounced until a 4 wt % CNC
512 concentration, and much weaker for concentrations above this
513 value. Moreover, the fits show differences with the data in the
514 small q range (see individual fits in the SI, Figure S9). This is
515 probably due to the fact that the isotropic-to-nematic phase
516 transition is reached at a concentration above 4 wt %, and the
517 suspensions are biphasic with liquid-crystalline and isotropic
518 regions.⁶⁰ This will be further discussed in the rheology
519 section. 520

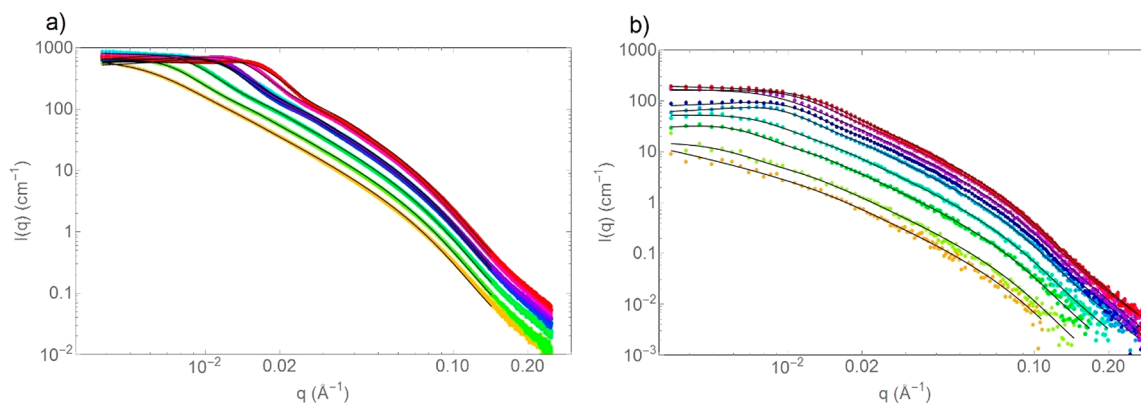


Figure 5. SAXS patterns, $I(q)$ versus q , in absolute scaling for (a) unmodified CNC suspensions (from Diamond) and (b) C₈-CNC (Ganesha) at various concentrations. The fits made using the model of rigid interacting cylinders are given as solid black lines. The same patterns are plotted individually in Figures S9 and S10 in the SI. Data measured at Diamond for C₈-CNC were also recorded for low concentrations and are given in Figure S11.

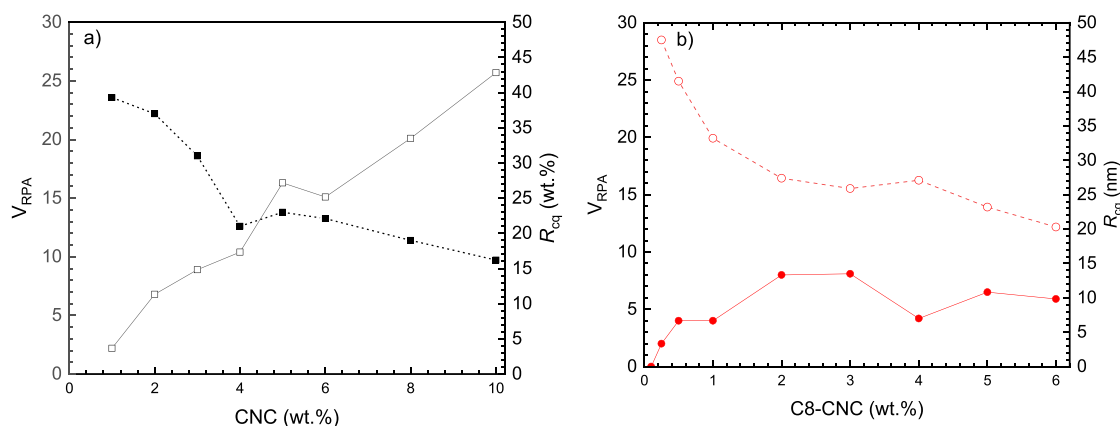


Figure 6. Influence of CNC concentration on ν_{RPA} (filled symbols) and R_{cq} (open symbols) determined from SAXS experiments for unmodified (a) CNCs and (b) C_8 -CNC. The lines are a guide to the eye.

To study the effect of CNC surface modification, C_8 -CNC suspensions were also characterized by SAXS at various concentrations (0.1–6 wt %) (Figure 5b). From the fit in the dilute regime (0.1 wt %), where the signal is attributed to isolated CNCs with negligible interactions, the form factor of the particles can be extracted. The cross-section of the rods is found to be $R_{\text{min}} = 1.6 \pm 0.1$ nm and $R_{\text{max}} = 9.2 \pm 0.1$ nm for the minor and major radii, respectively. Modification of the CNC induced a significant reduction in the major radius compared to unmodified CNCs. Above 0.25 wt %, interactions between C_8 -CNCs are needed to fit the data. Interestingly, in opposition to unmodified CNC, ν_{RPA} increases only up to ca. 2 wt % (with slightly stronger repulsion for C_8 -CNC than their unmodified counterparts at 1 and 2 wt %). Above 2 wt %, ν_{RPA} remains relatively constant. A similar trend is observed for R_{cq} , which strongly decreases up to 2 wt %, before stabilizing, or only weakly decreasing, to reach 20 nm at 6 wt %. The rapid stabilization of the repulsion forces in the system around ca. 2 wt % corresponds to the concentration at which an invertible gel is formed with C_8 -CNC (SI, Figure S12). Hence, this trend could be explained by the formation of the self-standing gel, with a network spanning throughout the entire suspension, with contact points between CNCs at larger dimensions than probed in this q -range formed between C_8 -CNC nanorods due to hydrophobic effects. This would “freeze” the C_8 -CNC in a disordered fashion, preventing the formation of a nematic phase.

Rheological Properties of CNC Suspensions. The rheological properties of aqueous suspensions of CNCs produced by hydrolysis with sulfuric acid have been previously characterized in detail.^{54,60–63} These previously published works also covered suspensions of CNCs of the same source as used in our study.⁶³ It is generally agreed that the rheological properties of suspensions of unmodified CNCs are defined by their ability to form biphasic systems of isotropic and chiral nematic phases. CNC suspensions exhibit Newtonian fluid behavior at low concentrations when suspensions are isotropic. However, at higher concentrations, CNCs form a liquid crystalline phase transforming the suspension into a biphasic system with the liquid crystal phase fraction being dependent on CNC concentration. These structural changes transform the suspensions into viscoelastic fluids. Ultimately, at sufficiently high concentrations, randomly entangled gels are formed. The aspect ratio and surface charge of the rodlike cellulose nanoparticles and the ionic strength of the aqueous

media determine the critical concentrations for the transitions between these states.

The rheological properties of hydrophobized and unmodified CNCs were investigated at a wide range of concentrations, which covered systems from fluids to gels. Our results for unmodified CNCs are in good agreement with previous findings^{54,60–63} as outlined above. For example, frequency sweeps in oscillatory rheology demonstrated that suspensions of unmodified CNCs exhibited liquidlike behavior ($G'' > G'$) for CNC concentrations < 5 wt % (SI, Figure S13a). When concentrations exceeded 5 wt %, elastic properties became dominant ($G' > G''$). Hydrophobization of CNCs drastically changed the viscoelastic properties, significantly increasing values of G' (SI, Figure S13b–d). Dominance of elastic properties ($G' > G''$) was extended to the suspensions with concentrations as low as 1 wt % for C_8 -CNCs and C_{12} -CNCs but only to 4 wt % for C_6 -CNCs. Interestingly, values of G' were larger than G'' for suspensions of hydrophobized CNCs that did not form invertible gels (concentrations forming invertible gels were 1.5, 2.5, and 4 wt % for C_{12} -, C_8 -, and C_6 -CNCs respectively; SI, Figure S12). For suspensions at concentrations below the invertible gel concentration, differences in G' and G'' were less than a decade ($\tan \delta \approx 0.1$). These values are characteristic for “weak gels” or “structured fluids” which are usually formed by tenuous association of mesoscopic domains.⁶⁴

The frequency dependence of the storage modulus was analyzed quantitatively by fitting a simple power law relationship, according to the equation

$$G' \propto \omega^p \quad (2)$$

where ω is the angular frequency of oscillation, and p is the storage modulus power law index.

There were only slight variations in the power law index in the studied range of concentrations for C_8 -CNCs and C_{12} -CNCs. For C_8 -CNCs, p decreased slightly from 0.09 for a 1 wt % C_8 -CNC suspension to 0.07 for 7 wt %, while p was 0.06 for 1 wt % C_{12} -CNCs and was constant (ca. 0.04) for concentrations between 2 and 5 wt %. Thus, the frequency independence of G' was observed even for suspensions at the lowest concentrations of C_8 -CNCs and C_{12} -CNCs. However, for C_6 -CNCs, G' was strongly dependent on frequency for the suspensions with concentrations between 2 and 4 wt % (p was ca. 2, 0.7, and 0.12 for 2, 3, and 4 wt %, respectively). A

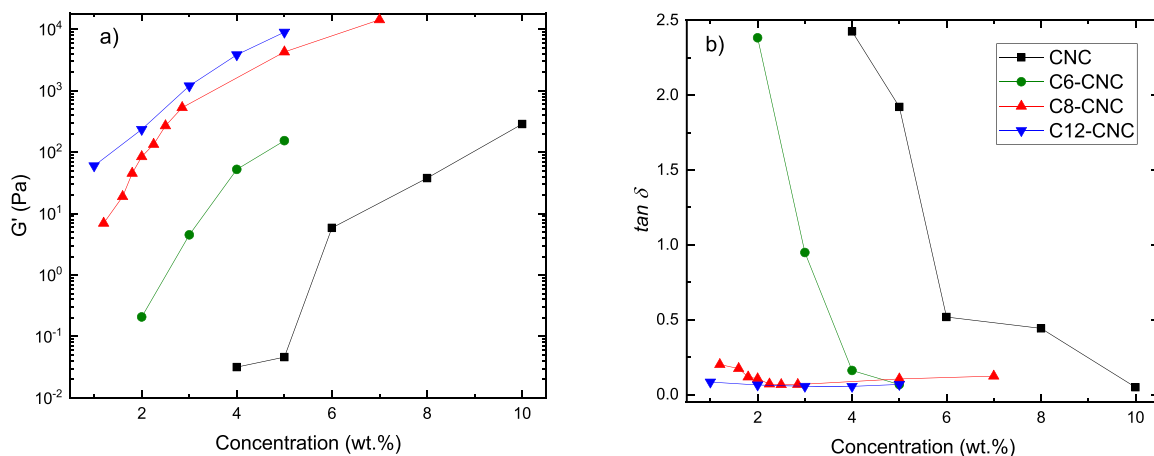


Figure 7. (a) Storage modulus and (b) $\tan \delta$ as a function of concentration of unmodified and hydrophobized CNCs at an angular frequency of 6.34 rad s^{-1} and strain 1.5%.

609 frequency independent G' was only observed for C_6 -CNC
610 suspensions when concentration exceeded 5 wt %.

611 The viscoelastic properties of unmodified and hydro-
612 phobized CNCs were compared at different CNC concen-
613 trations (Figure 7). As expected, G' increased with
614 concentration for all CNCs. However, rheological properties
615 are strongly dependent on the hydrophobicity of CNCs, and
616 suspensions and gels of C_8 - and C_{12} -CNCs exhibited
617 significantly higher G' values compared with suspensions of
618 unmodified CNCs and C_6 -CNCs at the same concentration.
619 For example, at 5 wt %, the G' value of an C_8 -CNC gel
620 suspension is higher than for unmodified CNCs by almost 5
621 orders of magnitude, with values of 4300 and 0.05 Pa,
622 respectively. G' increased further to ~ 9000 Pa for 5 wt %
623 C_{12} -CNCs. Modification with the shorter chain hexylamine
624 resulted in a moderate increase in G' to ca. 150 Pa for 5 wt %
625 C_6 -CNCs. Also, a strong dependence of $\tan \delta$ on
626 concentration was observed for unmodified CNC and C_6 -
627 CNC suspensions while $\tan \delta$ was below 1.08 for the complete
628 concentration range for C_8 - and C_{12} -CNCs (Figure 7b). The
629 elastic properties of unmodified CNC and C_6 -CNC
630 suspensions only became significant when concentrations
631 exceeded 5 and 3 wt %, respectively. When the concentrations
632 increased beyond these points $\tan \delta$ fell below 1.0 which is
633 usually attributed to gel formation. However, self-supported
634 gels (invertible gels) are not formed when $\tan \delta$ is equal to 1.0
635 at CNC concentrations 3 wt % for C_6 -CNCs and 5 wt % for
636 unmodified CNCs (SI, Figure S12).

637 It is well-known that the gel formation of CNC suspensions
638 can be induced by the introduction of electrolytes.^{54,63,65} Such
639 behavior has been observed for suspensions of charged
640 particles other than CNCs and attributed to the aggregation
641 of these particles with an increase in ionic strength. Viscoelastic
642 properties of CNCs were hence also compared for suspensions
643 prepared in 0.1 M KCl at a CNC concentration of 4 wt %
644 (Figure 8). The presence of electrolyte induced a significant
645 increase in G' for unmodified CNCs, and G' became larger
646 than G'' ($\tan \delta$ around 0.1 compared with 2.0 in the absence of
647 salt). Suspensions of hydrophobized CNCs are characterized
648 by higher G' compared with unmodified CNCs. However,
649 unlike the suspensions in DI water, there was no direct
650 correlation with the number of carbon atoms of alkyl chain
651 (hydrophobicity) and G' values of suspensions with back-
652 ground electrolyte: G' values for C_{12} -CNC suspension were

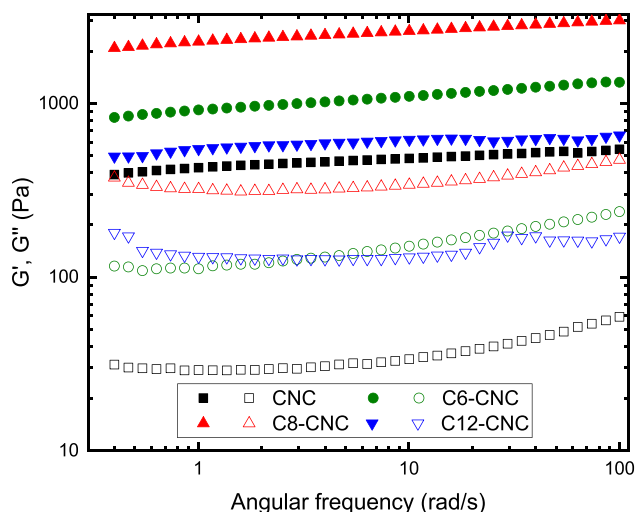


Figure 8. Dependence of storage modulus (filled symbols) and loss modulus (open symbols) on oscillation frequency of gels of unmodified and hydrophobized CNCs at 4 wt % in 0.1 M KCl. Strain 1.5%.

653 lower compared with values for the suspensions of C_8 -CNCs
654 and C_6 -CNCs. In fact, G' values for C_{12} -CNCs suspensions
655 in 0.1 KCl were lower than in DI water while the background
656 electrolyte induced an increase in G' values for C_6 - and C_8 -
657 CNC suspensions. It should be noted that hydrophobic effects
658 in hydrophobized CNCs had more pronounced influence on
659 CNC rheology compared with the electrolyte effect. For
660 example, at an angular frequency 6.34 rad s^{-1} , G' of 5 wt %
661 C_8 -CNC suspension in DI water was 4300 Pa in comparison
662 with 880 Pa for 5 wt % suspension of unmodified CNCs in 0.1
663 M KCl solutions.

664 As was discussed in previous sections, surface functionaliza-
665 tion of CNCs with hydrophobic moieties facilitates inter-
666 actions between CNCs due to hydrophobic effects. Therefore,
667 the formation of microgel aggregates is thought to occur even
668 at relatively low concentrations of hydrophobized CNCs,
669 especially for the more hydrophobic C_8 - and C_{12} -CNCs,
670 leading to phase separation. The elastic behavior of such a
671 weak gel is caused by the elasticity of the hydrophobized CNC
672 microgel dispersed in the aqueous phase depleted of CNCs.
673 However, such a system does not form self-supporting gels.

674 With an increase in concentration of hydrophobized CNCs, a
 675 strong network of connected aggregates is formed, leading to
 676 strong gels. It is worth noting that electrolytes have strong
 677 effects on the rheological properties and gelation of hydro-
 678 phobized CNCs. Therefore, structural and rheological proper-
 679 ties of hydrophobized CNCs are defined by two competing
 680 phenomena: electrostatic repulsion and association driven by
 681 hydrophobic effects. Under different conditions (CNC and
 682 electrolyte concentrations, hydrophobicity of modifying agent)
 683 one phenomenon can prevail over the other; for example,
 684 electrostatic repulsion is suppressed at higher ionic stress
 685 leading to the dominance of the hydrophobic effect. This is
 686 probably the reason for the decreased elastic properties of
 687 C_{12} -CNC gels in the presence of a background electrolyte
 688 (Figure 8). For these most hydrophobic CNCs, when
 689 electrostatic repulsion is suppressed the hydrophobic effect
 690 became too strong, inducing excessive C_{12} -CNC aggregation.
 691 As a result, G' is lower in the presence of electrolyte than in
 692 C_{12} -CNCs hydrogel prepared in DI water. At the same time,
 693 G' increased in the presence of KCl for C_6 - and C_8 -CNCs.
 694 Gel formation was also observed at slightly higher concen-
 695 trations of hydrophobized CNCs in 0.1 M KCl compared with
 696 suspensions in DI water (data not shown). Thus, at relatively
 697 low concentrations of hydrophobized CNCs, the addition of
 698 electrolytes disrupted the network, causing the formation of a
 699 phase-separated system. These observations indicate that the
 700 surface charge contributes to the stabilization of the network
 701 formed via the CNC association driven by hydrophobic effects.
 702 Rheological properties of CNC suspensions/gels were
 703 further characterized in steady-shear experiments (SI, Figure
 704 S14). The pattern of the response of unmodified CNC
 705 suspensions/gels to shear flow (SI, Figure S14a) was similar to
 706 previous independent studies.^{54,61,62} At CNC concentrations
 707 sufficiently high for forming biphasic systems, there are three
 708 regions in the flow curve (for example, curves for 5 and 6 wt %
 709 in Figure S14a). The low shear rate region presents a strong
 710 shear thinning behavior. It is followed by the region with a
 711 weak dependence of the viscosity on shear rate and another
 712 shear-thinning region at higher shear rates. The three-region
 713 pattern has been also previously reported for other liquid
 714 crystal systems.^{66,67} For CNCs it is generally agreed that the
 715 first shear thinning region is caused by alignment of the
 716 nematic liquid crystalline domains. When alignment of these
 717 domains is completed, an increase in shear rate destabilizes the
 718 nematic mesophase, which manifests as weak dependences of
 719 viscosity on shear rate. Finally, at high shear rates, shear
 720 thinning is due to alignment of the CNC nanorods. Different
 721 regions of viscosity sensitivity to the shear rate were observed
 722 at some concentrations only for C_8 - and C_{12} -CNCs (SI,
 723 Figure S14c,d). However, only one regime of shear thinning
 724 was observed for C_6 -CNCs suspension/gels in the studied
 725 range of concentrations. A set of viscosity values at various
 726 concentrations was extracted from flow curves for a shear rate
 727 of 0.1 s^{-1} and presented in Figure 9. In agreement with the
 728 results from oscillatory rheology experiments, viscosities of the
 729 gels based on hydrophobized CNCs are significantly higher
 730 than unmodified CNCs. For example, for systems containing 4
 731 wt % of CNCs, shear viscosity increased from 0.07 Pa s for
 732 unmodified CNCs to ca. 1350 Pa s in the case of C_{12} -CNCs.
 733 There was a direct correlation between hydrophobicity of
 734 CNCs (length of alkyl radical) and enhancement in viscosity
 735 (unmodified CNCs < C_6 -CNCs < C_8 -CNCs < C_{12} -CNCs).

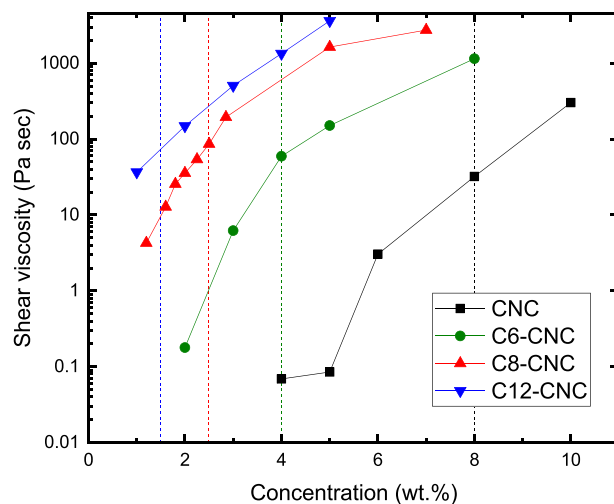


Figure 9. Dependence of steady flow viscosity of unmodified and hydrophobized CNC suspensions/gels in deionized water on CNC concentrations at a shear rate of 0.1 s^{-1} . Vertical lines indicate concentrations for forming invertible gels (the color of the lines matches with the color of symbols for the corresponding experimental points).

Dependence of the viscosity on concentration has been
 proposed as a means for the identification of the transition of
 aqueous CNC systems from isotropic to biphasic.⁶⁰ The region
 of a sharp increase of viscosity indicates transformation of the
 system into a biphasic system. For CNCs used in this study
 this occurred at a concentration around 5 wt % (Figure 9).
 Thus, quite high concentrations of CNCs used in this study are
 required to enable assembly into structured liquid crystalline
 domains. Figure 9 also shows concentrations corresponding to
 the formation of invertible gels. These concentrations for
 hydrophobized CNCs (1.5, 2.5, and 4 wt % for C_{12} -, C_8 -, and
 C_6 -CNCs, respectively) are lower than the concentration of
 the transition into biphasic phase for unmodified CNCs. This
 might impede the formation of liquid crystalline phases in the
 suspensions of hydrophobized CNCs, which agrees with the
 C_8 -CNC SAXS data (no obvious variation of the interactions
 for concentrations above the formation of an invertible gel).
 To check the formation of a liquid crystalline phase,
 microscopic images in cross-polarized light of the suspensions
 were obtained (SI, Figure S15). Formation of liquid crystalline
 domains was confirmed for unmodified CNCs. However, all
 hydrophobized CNCs did not exhibit birefringence, confirming
 no formation of a liquid crystalline phase at concentrations
 below and above gel formation, again in agreement with the
 weak repulsive interaction observed in SAXS. Random
 association of hydrophobized CNCs arresting the CNC
 mobility in the gel state prevents the formation of a liquid
 crystalline phase. Earlier inhibition of the formation of ordered
 liquid crystalline structures due to gelation was assumed for the
 systems based on cationically modified CNCs.⁶⁸ Although the
 three-region pattern of flow curves was observed for some
 concentrations of C_8 - and C_{12} -CNCs, similar to the pattern
 characteristic for unmodified CNCs (SI, Figure S14), the
 underlying structural changes are different for these materials.
 We suggest that the first shear thinning region is related to
 defragmentation of a network formed by small aggregates of
 hydrophobized CNCs. In the second region aggregates are
 disassembled into individual nanorods or stacks of few

774 nanorods. At high shear rates, shear thinning is caused by the
775 alignment of redispersed CNCs.

776 ■ CONCLUSIONS

777 CNCs have been modified with alkylamines of different lengths
778 (C6, C8, and C12) to vary the hydrophilic–hydrophobic
779 balance. The properties of aqueous colloidal systems with
780 hydrophobized CNCs have been studied particularly to assess
781 the impact of hydrophobic effects on CNC association and
782 gelation in aqueous media. We have demonstrated that
783 hydrophobicity of modified CNCs correlated with the chain
784 lengths of alkylamines. Although a two-stage modification
785 process based on reductive amination led to a decrease in the
786 content of surface sulfate half-esters, at least half of this ionic
787 group was preserved providing a good colloidal stability of
788 hydrophobized CNCs. Thus, the surface of modified CNCs
789 contained both hydrophilic and hydrophobic domains. As a
790 result, the modified CNCs are surface active nanoparticles
791 demonstrating amphiphilic properties. However, there ap-
792 peared to be no direct correlation between the length of alkyl
793 chain attached to the CNC surface and surface activity; C₁₂-
794 CNCs induced a smaller decrease in interfacial tension than
795 C₈-CNCs which was attributed to stronger association driven
796 by hydrophobic effects. Self-association of hydrophobized
797 CNCs was confirmed by SAXS and autofluorescent spectroscopy
798 experiments. Formation of transient networks by
799 hydrophobized CNCs due to this self-association induces
800 changes in gelation and rheological properties of CNC
801 suspensions. Critical concentrations of sol/gel transitions for
802 hydrophobized CNC are significantly lower than the hydro-
803 philic CNCs and depend on hydrophobicity of modified
804 CNCs. Self-association of hydrophobic CNCs results in
805 stronger, more rigid gels. Our work highlights the versatility
806 and efficiency of modifying rheological properties of aqueous
807 systems via self-association of hydrophobized CNCs.

808 ■ ASSOCIATED CONTENT

809 **SI** Supporting Information

810 The Supporting Information is available free of charge at
811 <https://pubs.acs.org/doi/10.1021/acs.biomac.9b01721>.

812 Solid state NMR spectra and peak deconvolution;
813 Raman spectrum of oxidized CNCs; pictures of sessile
814 drops on surfaces of unmodified and hydrophobized
815 CNCs films; results of multichannel confocal laser
816 scanning spectroscopy; results of SAXS experiments;
817 pictures of unmodified and hydrophobized CNC
818 suspensions of different concentrations; rheology results
819 for aqueous suspensions/gels; and images of gels in
820 cross-polarized light (PDF)

821 ■ AUTHOR INFORMATION

822 Corresponding Authors

823 **Rinat Nigmatullin** – Department of Aerospace Engineering,
824 Bristol Composites Institute (ACCIS), University of Bristol,
825 Bristol BS8 1TR, United Kingdom; Email: [rn17541@](mailto:rn17541@bristol.ac.uk)
826 bristol.ac.uk

827 **Stephen J. Eichhorn** – Department of Aerospace Engineering,
828 Bristol Composites Institute (ACCIS), University of Bristol,
829 Bristol BS8 1TR, United Kingdom; [orcid.org/0000-0003-](https://orcid.org/0000-0003-4101-273X)
830 [4101-273X](https://orcid.org/0000-0003-4101-273X); Email: s.j.eichhorn@bristol.ac.uk

831 Authors

Marcus A. Johns – Department of Aerospace Engineering,
832 Bristol Composites Institute (ACCIS), University of Bristol,
833 Bristol BS8 1TR, United Kingdom 834
Juan C. Muñoz-García – School of Pharmacy, University of
835 East Anglia, Norwich NR4 7TJ, United Kingdom; 836
orcid.org/0000-0003-2246-3236 837
Valeria Gabrielli – School of Pharmacy, University of East
838 Anglia, Norwich NR4 7TJ, United Kingdom 839
Julien Schmitt – Department of Chemistry, University of Bath,
840 Bath BA2 7AY, United Kingdom; LSFC—Laboratoire de
841 Synthèse et Fonctionnalisation des Céramiques UMR 3080
842 CNRS/Saint-Gobain CREE, Saint-Gobain Research Provence,
843 Cavailon 84300, France; orcid.org/0000-0002-3452-6655 844
Jesús Angulo – School of Pharmacy, University of East Anglia,
845 Norwich NR4 7TJ, United Kingdom 846
Yaroslav Z. Khimyak – School of Pharmacy, University of East
847 Anglia, Norwich NR4 7TJ, United Kingdom; [orcid.org/](https://orcid.org/0000-0003-0424-4128)
848 [0000-0003-0424-4128](https://orcid.org/0000-0003-0424-4128) 849
Janet L. Scott – Department of Chemistry, University of Bath,
850 Bath BA2 7AY, United Kingdom; [orcid.org/0000-0001-](https://orcid.org/0000-0001-8021-2860)
851 [8021-2860](https://orcid.org/0000-0001-8021-2860) 852
Karen J. Edler – Department of Chemistry, University of Bath,
853 Bath BA2 7AY, United Kingdom; [orcid.org/0000-0001-](https://orcid.org/0000-0001-5822-0127)
854 [5822-0127](https://orcid.org/0000-0001-5822-0127) 855

856 Complete contact information is available at: 856
857 <https://pubs.acs.org/doi/10.1021/acs.biomac.9b01721> 857

858 Author Contributions

859 The manuscript was written through contributions of all 859
860 authors led by R.N. and S.J.E. All authors have given approval 860
861 to the final version of the manuscript. 861

862 Funding

863 The Engineering and Physical Sciences Research Council 863
864 (EPSRC) is acknowledged for provision of financial support 864
865 (EP/N03340X/2, EP/N033337/1) for J.C.M.-G., J.A., and 865
866 Y.Z.K. 866

867 Notes

868 The authors declare no competing financial interest. 868

869 ■ ACKNOWLEDGMENTS

870 The authors gratefully acknowledge the KRÜSS Surface 870
871 Science Centre (KSSC) at the University of Bristol and the 871
872 Material and Chemical Characterization Facility (MC2) at the 872
873 University of Bath (<http://go.bath.ac.uk/mc2>) for access to 873
874 research equipment and assistance in this work. Dr. Nick Terril 874
875 and Dr. Andrew Smith on beamline I22 are thanked for 875
876 assistance with SAXS experiments at Diamond Light Source 876
877 Ltd (experiments no. SM17580-1). Prof. Robert Richardson is 877
878 thanked for his help with SAXS measurements on the Ganesha. 878
879 We are also grateful for the UEA Faculty of Science NMR 879
880 facility. V.G. would like to acknowledge the support of BBSRC 880
881 Norwich Research Park Bioscience Doctoral Training Grant 881
882 (BB/M011216/1). 882

883 ■ ABBREVIATIONS

884 CAC, critical aggregation concentration; CNC, cellulose 884
885 nanocrystal; CNM, cellulose nanomaterial; DI, deionized; 885
886 LVE, linear viscoelastic; MCLSS, multichannel confocal laser 886
887 scanning spectroscopy; SAXS, small-angle X-ray scattering 887

888 ■ REFERENCES

- 889 (1) Stark, W. J.; Stoessel, P. R.; Wohlleben, W.; Hafner, A. Industrial
890 applications of nanoparticles. *Chem. Soc. Rev.* **2015**, *44* (16), 5793–
891 5805.
- 892 (2) Heiligtag, F. J.; Niederberger, M. The fascinating world of
893 nanoparticle research. *Mater. Today* **2013**, *16* (7), 262–271.
- 894 (3) Jutz, G.; Böker, A. Bionanoparticles as functional macro-
895 molecular building blocks – A new class of nanomaterials. *Polymer*
896 **2011**, *52* (2), 211–232.
- 897 (4) Lin, N.; Huang, J.; Dufresne, A. Preparation, properties and
898 applications of polysaccharide nanocrystals in advanced functional
899 nanomaterials: a review. *Nanoscale* **2012**, *4* (11), 3274–3294.
- 900 (5) Klemm, D.; Kramer, F.; Moritz, S.; Lindström, T.; Ankerfors,
901 M.; Gray, D.; Dorris, A. Nanocelluloses: A new family of nature-based
902 materials. *Angew. Chem., Int. Ed.* **2011**, *50* (24), 5438–5466.
- 903 (6) Abitbol, T.; Rivkin, A.; Cao, Y.; Nevo, Y.; Abraham, E.; Ben-
904 Shalom, T.; Lapidot, S.; Shoseyov, O. Nanocellulose, a tiny fiber with
905 huge applications. *Curr. Opin. Biotechnol.* **2016**, *39*, 76–88.
- 906 (7) Gang, O. Nanoparticle assembly: from fundamentals to
907 applications: concluding remarks. *Faraday Discuss.* **2016**, *186*, 529–
908 537.
- 909 (8) Grzelczak, M.; Vermant, J.; Furst, E. M.; Liz-Marzán, L. M.
910 Directed self-assembly of nanoparticles. *ACS Nano* **2010**, *4* (7),
911 3591–3605.
- 912 (9) Li, F.; Lu, J.; Kong, X.; Hyeon, T.; Ling, D. Dynamic
913 nanoparticle assemblies for biomedical applications. *Adv. Mater.*
914 **2017**, *29* (14), 1605897.
- 915 (10) Gray, D.; Mu, X. Chiral nematic structure of cellulose
916 nanocrystal suspensions and films; Polarized light and atomic force
917 microscopy. *Materials* **2015**, *8* (11), 7873.
- 918 (11) Capron, I.; Rojas, O. J.; Bordes, R. Behavior of nanocelluloses
919 at interfaces. *Curr. Opin. Colloid Interface Sci.* **2017**, *29*, 83–95.
- 920 (12) Eyley, S.; Thielemans, W. Surface modification of cellulose
921 nanocrystals. *Nanoscale* **2014**, *6* (14), 7764–7779.
- 922 (13) Habibi, Y. Key advances in the chemical modification of
923 nanocelluloses. *Chem. Soc. Rev.* **2014**, *43* (5), 1519–1542.
- 924 (14) Goussé, C.; Chanzy, H.; Excoffier, G.; Soubeyrand, L.; Fleury,
925 E. Stable suspensions of partially silylated cellulose whiskers dispersed
926 in organic solvents. *Polymer* **2002**, *43* (9), 2645–2651.
- 927 (15) Goussé, C.; Chanzy, H.; Cerrada, M. L.; Fleury, E. Surface
928 silylation of cellulose microfibrils: preparation and rheological
929 properties. *Polymer* **2004**, *45* (5), 1569–1575.
- 930 (16) Andresen, M.; Johansson, L.-S.; Tanem, B. S.; Stenius, P.
931 Properties and characterization of hydrophobized microfibrillated
932 cellulose. *Cellulose* **2006**, *13* (6), 665–677.
- 933 (17) Cunha, A. G.; Mougel, J.-B.; Cathala, B.; Berglund, L. A.;
934 Capron, I. Preparation of double pickeringemulsions stabilized by
935 chemically tailored nanocelluloses. *Langmuir* **2014**, *30* (31), 9327–
936 9335.
- 937 (18) Sojoudiasli, H.; Heuzey, M.-C.; Carreau, P. J.; Riedl, B.
938 Rheological behavior of suspensions of modified and unmodified
939 cellulose nanocrystals in dimethyl sulfoxide. *Rheol. Acta* **2017**, *56* (7),
940 673–682.
- 941 (19) Siqueira, G.; Bras, J.; Dufresne, A. Cellulose whiskers versus
942 microfibrils: Influence of the nature of the nanoparticle and its surface
943 functionalization on the thermal and mechanical properties of
944 nanocomposites. *Biomacromolecules* **2009**, *10* (2), 425–432.
- 945 (20) Shang, W.; Huang, J.; Luo, H.; Chang, P. R.; Feng, J.; Xie, G.
946 Hydrophobic modification of cellulose nanocrystal via covalently
947 grafting of castor oil. *Cellulose* **2013**, *20* (1), 179–190.
- 948 (21) Lee, Y. R.; Park, D.; Choi, S. K.; Kim, M.; Baek, H. S.; Nam, J.;
949 Chung, C. B.; Osuji, C. O.; Kim, J. W. Smart cellulose nanofluids
950 produced by tunable hydrophobic association of polymer-grafted
951 cellulose nanocrystals. *ACS Appl. Mater. Interfaces* **2017**, *9* (36),
952 31095–31101.
- 953 (22) Yoo, Y.; Youngblood, J. P. Green one-pot synthesis of surface
954 hydrophobized cellulose nanocrystals in aqueous medium. *ACS*
955 *Sustainable Chem. Eng.* **2016**, *4* (7), 3927–3938.
- (23) Shimizu, M.; Saito, T.; Fukuzumi, H.; Isogai, A. Hydrophobic, 956
ductile, and transparent nanocellulose films with quaternary 957
alkylammonium carboxylates on nanofibril surfaces. *Biomacromolecules* 958
2014, *15* (11), 4320–4325. 959
- (24) Salajkova, M.; Berglund, L. A.; Zhou, Q. Hydrophobic cellulose 960
nanocrystals modified with quaternary ammonium salts. *J. Mater.* 961
Chem. **2012**, *22* (37), 19798–19805. 962
- (25) Shimizu, M.; Saito, T.; Isogai, A. Bulky quaternary 963
alkylammonium counterions enhance the nanodispersibility of 964
2,2,6,6-tetramethylpiperidine-1-oxyl-oxidized cellulose in diverse 965
solvents. *Biomacromolecules* **2014**, *15* (5), 1904–1909. 966
- (26) Ansari, F.; Salajková, M.; Zhou, Q.; Berglund, L. A. Strong 967
surface treatment effects on reinforcement efficiency in biocompos- 968
itesbased on cellulose nanocrystals in oly(vinyl acetate) matrix. 969
Biomacromolecules **2015**, *16* (12), 3916–3924. 970
- (27) Cervin, N. T.; Johansson, E.; Benjamins, J.-W.; Wågberg, L. 971
Mechanisms behind the stabilizing action of cellulose nanofibrils in 972
wet-stable cellulose foams. *Biomacromolecules* **2015**, *16* (3), 822–831. 973
- (28) Kedzior, S. A.; Marway, H. S.; Cranston, E. D. Tailoring 974
cellulose nanocrystal and surfactant behavior in miniemulsionpolyme- 975
rization. *Macromolecules* **2017**, *50* (7), 2645–2655. 976
- (29) Saidane, D.; Perrin, E.; Cherhal, F.; Guellec, F.; Capron, I. 977
Some modification of cellulose nanocrystals for functional Pickering 978
emulsions. *Philos. Trans. R. Soc., A* **2016**, *374* (2072), 20150139. 979
- (30) Wei, Z.; Sinko, R.; Ketten, S.; Luijten, E. Effect of surface 980
modification on water adsorption and interfacial mechanics of 981
cellulose nanocrystals. *ACS Appl. Mater. Interfaces* **2018**, *10* (9), 982
8349–8358. 983
- (31) Hu, Z.; Ballinger, S.; Pelton, R.; Cranston, E. D. Surfactant- 984
enhanced cellulose nanocrystal Pickering emulsions. *J. Colloid* 985
Interface Sci. **2015**, *439*, 139–148. 986
- (32) Fox, D. M.; Rodriguez, R. S.; Devilbiss, M. N.; Woodcock, J.; 987
Davis, C. S.; Sinko, R.; Ketten, S.; Gilman, J. W. Simultaneously 988
tailoring surface energies and thermal stabilities of cellulose 989
nanocrystals using ion exchange: Effects on polymer composite 990
properties for transportation, infrastructure, and renewable energy 991
applications. *ACS Appl. Mater. Interfaces* **2016**, *8* (40), 27270–27281. 992
- (33) Dhar, N.; Au, D.; Berry, R. C.; Tam, K. C. Interactions of 993
nanocrystalline cellulose with an oppositely charged surfactant in 994
aqueous medium. *Colloids Surf., A* **2012**, *415*, 310–319. 995
- (34) Brinatti, C.; Uang, J.; Berry, R. M.; Tam, K. C.; Loh, W. 996
Structural and energetic studies on the interaction of cationic 997
surfactants and cellulose nanocrystals. *Langmuir* **2016**, *32* (3), 689– 998
698. 999
- (35) Dash, R.; Elder, T.; Ragauskas, A. J. Grafting of model primary 1000
amine compounds to cellulose nanowhiskers through periodate 1001
oxidation. *Cellulose* **2012**, *19* (6), 2069–2079. 1002
- (36) Ojala, J.; Sirviö, J. A.; Liimatainen, H. Nanoparticle emulsifiers 1003
based on bifunctionalized cellulose nanocrystals as marine diesel oil– 1004
water emulsion stabilizers. *Chem. Eng. J.* **2016**, *288*, 312–320. 1005
- (37) Visanko, M.; Liimatainen, H.; Sirviö, J. A.; Heiskanen, J. P.; 1006
Niimäki, J.; Hormi, O. Amphiphilic cellulose nanocrystals from acid- 1007
free oxidative treatment: Physicochemical characteristics and use as an 1008
oil–water stabilizer. *Biomacromolecules* **2014**, *15* (7), 2769–2775. 1009
- (38) Tang, C.; Spinney, S. B.; Shi, Z.; Tang, J.; Peng, B.; Luo, J.; 1010
Tam, K. C. Amphiphilic cellulose nanocrystals for enhanced Pickering 1011
emulsion stabilization. *Langmuir* **2018**, *34* (43), 12897–12905. 1012
- (39) Hu, Z.; Berry, R. M.; Pelton, R.; Cranston, E. D. One-pot 1013
water-based hydrophobic surface modification of cellulose nanocrystal- 1014
s using plant polyphenols. *ACS Sustainable Chem. Eng.* **2017**, *5* (6), 1015
5018–5026. 1016
- (40) Lee, K.-Y.; Aitomäki, Y.; Berglund, L. A.; Oksman, K.; 1017
Bismarck, A. On the use of nanocellulose as reinforcement in polymer 1018
matrix composites. *Compos. Sci. Technol.* **2014**, *105*, 15–27. 1019
- (41) Chen, J.; Lin, N.; Huang, J.; Dufresne, A. Highly alkynyl- 1020
functionalization of cellulose nanocrystals and advanced nano- 1021
composites thereof via click chemistry. *Polym. Chem.* **2015**, *6* (24), 1022
4385–4395. 1023

- 1024 (42) Gan, L.; Liao, J.; Lin, N.; Hu, C.; Wang, H.; Huang, J. Focus on
1025 gradientwise control of the surface acetylation of cellulose nanocrystals
1026 to optimize mechanical reinforcement for hydrophobic polyester-
1027 based nanocomposites. *ACS Omega* **2017**, *2* (8), 4725–4736.
- 1028 (43) Peng, S. X.; Shrestha, S.; Yoo, Y.; Youngblood, J. P. Enhanced
1029 dispersion and properties of a two-component epoxy nanocomposite
1030 using surface modified cellulose nanocrystals. *Polymer* **2017**, *112*,
1031 359–368.
- 1032 (44) Palange, C.; Johns, M. A.; Scurr, D. J.; Phipps, J. S.; Eichhorn,
1033 S. J. The effect of the dispersion of microfibrillated cellulose on the
1034 mechanical properties of melt-compounded polypropylene–poly-
1035 ethylene copolymer. *Cellulose* **2019**, *26* (18), 9645–9659.
- 1036 (45) Chassenieux, C.; Nicolai, T.; Benyahia, L. Rheology of
1037 associative polymer solutions. *Curr. Opin. Colloid Interface Sci.* **2011**,
1038 *16* (1), 18–26.
- 1039 (46) Winnik, M. A.; Yekta, A. Associative polymers in aqueous
1040 solution. *Curr. Opin. Colloid Interface Sci.* **1997**, *2* (4), 424–436.
- 1041 (47) Wang, J.; Benyahia, L.; Chassenieux, C.; Tassin, J.-F.; Nicolai,
1042 T. Shear-induced gelation of associative polyelectrolytes. *Polymer*
1043 **2010**, *51* (9), 1964–1971.
- 1044 (48) Nigmatullin, R.; Harniman, R.; Gabrielli, V.; Muñoz-García, J.
1045 C.; Khimiyak, Y. Z.; Angulo, J.; Eichhorn, S. J. Mechanically robust
1046 gels formed from hydrophobized cellulose nanocrystals. *ACS Appl.*
1047 *Mater. Interfaces* **2018**, *10* (23), 19318–19322.
- 1048 (49) Nigmatullin, R.; Gabrielli, V.; Muñoz-García, J. C.;
1049 Lewandowska, A. E.; Harniman, R.; Khimiyak, Y. Z.; Angulo, J.;
1050 Eichhorn, S. J. Thermosensitive supramolecular and colloidal
1051 hydrogels via self-assembly modulated by hydrophobized cellulose
1052 nanocrystals. *Cellulose* **2019**, *26* (1), 529–542.
- 1053 (50) Larsson, P. T.; Wickholm, K.; Iversen, T. A CP/MAS13C
1054 NMR investigation of molecular ordering in celluloses. *Carbohydr.*
1055 *Res.* **1997**, *302* (1), 19–25.
- 1056 (51) Abitbol, T.; Kloser, E.; Gray, D. G. Estimation of the surface
1057 sulfur content of cellulose nanocrystals prepared by sulfuric acid
1058 hydrolysis. *Cellulose* **2013**, *20* (2), 785–794.
- 1059 (52) Schmitt, J.; Calabrese, V.; da Silva, M. A.; Lindhoud, S.;
1060 Alfredsson, V.; Scott, J. L.; Edler, K. J. TEMPO-oxidised cellulose
1061 nanofibrils; probing the mechanisms of gelation via small angle X-ray
1062 scattering. *Phys. Chem. Chem. Phys.* **2018**, *20* (23), 16012–16020.
- 1063 (53) Foster, E. J.; Moon, R. J.; Agarwal, U. P.; Bortner, M. J.; Bras, J.;
1064 Camarero-Espinosa, S.; Chan, K. J.; Clift, M. J. D.; Cranston, E. D.;
1065 Eichhorn, S. J.; Fox, D. M.; Hamad, W. Y.; Heux, L.; Jean, B.; Korey,
1066 M.; Nieh, W.; Ong, K. J.; Reid, M. S.; Renneckar, S.; Roberts, R.;
1067 Shatkin, J. A.; Simonsen, J.; Stinson-Bagby, K.; Wanasekara, N.;
1068 Youngblood, J. Current characterization methods for cellulose
1069 nanomaterials. *Chem. Soc. Rev.* **2018**, *47*, 2609–2679.
- 1070 (54) Oguzlu, H.; Danumah, C.; Boluk, Y. Colloidal behavior of
1071 aqueous cellulose nanocrystal suspensions. *Curr. Opin. Colloid*
1072 *Interface Sci.* **2017**, *29*, 46–56.
- 1073 (55) Reid, M. S.; Villalobos, M.; Cranston, E. D. Benchmarking
1074 cellulose nanocrystals: From the laboratory to industrial production.
1075 *Langmuir* **2017**, *33* (7), 1583–1598.
- 1076 (56) Chandar, P.; Somasundaran, P.; Turro, N. J. Fluorescence
1077 probe studies on the structure of the adsorbed layer of dodecyl sulfate
1078 at the alumina–water interface. *J. Colloid Interface Sci.* **1987**, *117* (1),
1079 31–46.
- 1080 (57) Misra, P. K.; Somasundaran, P. Fluorescence probing of the
1081 surfactant assemblies in solutions and at solid–liquid interfaces. In
1082 *Interfacial Processes and Molecular Aggregation of Surfactants*;
1083 Narayanan, R., Ed.; Springer Berlin Heidelberg: Berlin, Heidelberg,
1084 2008; pp 143–188.
- 1085 (58) Piñeiro, L.; Novo, M.; Al-Soufi, W. Fluorescence emission of
1086 pyrene in surfactant solutions. *Adv. Colloid Interface Sci.* **2015**, *215*, 1–
1087 12.
- 1088 (59) Johns, M. A.; Lewandowska, A. E.; Eichhorn, S. J. Rapid
1089 determination of the distribution of cellulose nanomaterial aggregates
1090 in composites enabled by multi-channel spectral confocal microscopy.
1091 *Microsc. Microanal.* **2019**, *25* (3), 682–689.
- (60) Ureña-Benavides, E. E.; Ao, G.; Davis, V. A.; Kitchens, C. L. 1092
Rheology and phase behavior of lyotropic cellulose nanocrystal 1093
suspensions. *Macromolecules* **2011**, *44* (22), 8990–8998. 1094
- (61) Shafiei-Sabet, S.; Hamad, W. Y.; Hatzikiriakos, S. G. Rheology 1095
of nanocrystalline cellulose aqueous suspensions. *Langmuir* **2012**, *28* 1096
(49), 17124–17133. 1097
- (62) Bercea, M.; Navard, P. Shear Dynamics of Aqueous 1098
Suspensions of Cellulose Whiskers. *Macromolecules* **2000**, *33* (16), 1099
6011–6016. 1100
- (63) Xu, Y.; Atrens, A. D.; Stokes, J. R. Rheology and microstructure 1101
of aqueous suspensions of nanocrystalline cellulose rods. *J. Colloid* 1102
Interface Sci. **2017**, *496*, 130–140. 1103
- (64) Picout, D. R.; Ross-Murphy, S. B. Rheology of biopolymer 1104
solutions and gels. *Sci. World J.* **2003**, *3*, 105–121. 1105
- (65) Phan-Xuan, T.; Thuresson, A.; Skepö, M.; Labrador, A.; 1106
Bordes, R.; Matic, A. Aggregation behavior of aqueous cellulose 1107
nanocrystals: the effect of inorganic salts. *Cellulose* **2016**, *23* (6), 1108
3653–3663. 1109
- (66) Hongladarom, K.; Burghardt, W. R. Molecular orientation, 1110
“Region I” shear thinning and the cholesteric phase in aqueous 1111
hydroxypropylcellulose under shear. *Rheol. Acta* **1998**, *37* (1), 46–53. 1112
- (67) Mewis, J.; Moldenaers, P. Rheology of polymeric liquid crystals. 1113
Curr. Opin. Colloid Interface Sci. **1996**, *1* (4), 466–471. 1114
- (68) Hasani, M.; Cranston, E. D.; Westman, G.; Gray, D. G. 1115
Cationic surface functionalization of cellulose nanocrystals. *Soft* 1116
Matter **2008**, *4* (11), 2238–2244. 1117